steel research international
www.steel-research.de

Increasing the Reuse Potential of High-Strength Steels by Extending the Fatigue Life through Surface Treatments

Ayush Shrivastava, Oguz Gulbay, Srinivasa Raghavan Raghuraman, Marion Kreins, Fabian Weber, Peter Starke, Alexander Gramlich, and Ulrich Krupp*

To enhance the circularity of engineering steels, this study investigates a surface reconditioning approach to extend the fatigue life of damaged tempered martensitic 42CrMo4 steel. Fatigue performance is evaluated through a four-phase methodology. In the first phase, specimens are cyclically loaded at 720 MPa and 5 Hz until 75% of their fatigue life is consumed, inducing high-cycle fatigue damage characterized by surface microcracks and subsurface persistent slip bands (PSBs). In the second phase, fatigue damage is analyzed using scanning electron microscopy, magnetic Barkhausen noise, and cross-sectional lamella extracted via plasma focused ion beam milling, revealing PSBs ≈5 µm below the surface. In the third phase, surface reconditioning through combined mechanical polishing and electropolishing is performed to remove about 100 µm of material and eliminate surface and near-surface damage. In the final phase, reconditioned specimens are retested at 630 MPa and 1000 Hz. Results show a 12-fold increase in fatigue life compared to non-reconditioned specimens; however, reconditioned specimens retain only about one-third of the fatigue life of pristine material. These findings demonstrate that surface reconditioning of fatigue-damaged steel significantly enhances remaining fatigue life and enable safe reuse, particularly in applications where surface-initiated damage governs failure.

1. Introduction

The popularity of steel across modern infrastructure, transportation, and manufacturing stems from its exceptional strength, durability, and recyclability. Steel production consumes large amounts of carbon and generates around 7% of worldwide CO_2 emissions, thus making it a major industrial factor in climate change.[1] The International Energy Agency (IEA) states that reaching net-zero emissions by 2050 depends on significant improvements in energy efficiency, low-carbon production methods, and circular economy concepts, which should include steel reuse as a key method to cut emissions and energy use.[2] The traditional recycling method for steel material circularity demands substantial energy for melting and refining processes before reshaping. Steel reuse maintains the original microstructure, reducing energy consumption by removing the need for reprocessing while producing an estimated 87% decrease in CO_2 emissions compared to recycling methods, as stated by Berglund-Brown.[3] Furthermore, by increasing the reuse share, the enrichment of recycling-introduced impurities will be slowed down, reducing their overall detrimental effect on steel performance.[4]

One of the major barriers to steel reuse is the uncertainty surrounding a component's prior service history, including loading conditions, environmental exposure, and accumulated damage. This lack of traceability raises concerns about hidden fatigue damage, which can compromise long-term performance and safety.[5] Moreover, the absence of standardized procedures to evaluate the residual fatigue life of reused components further limits their adoption.[6] Although fatigue failure typically progresses slowly, structural steel elements are frequently discarded prematurely, even when they retain sufficient structural integrity.[7] Research by Cooper et al. indicates that many steel elements undergo replacement before they achieve their full mechanical capabilities due to fatigue-related concerns, highlighting the potential of surface reconditioning techniques to extend service life.[8]

Steel undergoes progressive microstructural changes under repeated cyclic loading, including dislocation accumulation, localized plastic deformation, and eventual fatigue crack formation. According to Schijve, localized plasticity and interactions with

A. Shrivastava, O. Gulbay, M. Kreins, A. Gramlich, U. Krupp
IEHK Steel Institute
RWTH Aachen University
Intzestraße 1, 52072 Aachen, Germany
E-mail: ayush.shrivastava@iehk.rwth-aachen.de

S. R. Raghuraman, F. Weber, P. Starke
Department of Materials Science and Materials Testing (WWHK)
Institute QM³
University of Applied Sciences Kaiserslautern
Schoenstraße 11, 67657 Kaiserslautern, Germany

F. Weber, P. Starke
Faculty of Natural Sciences and Technology
Saarland University
66123 Saarbrücken, Germany

The ORCID identification number(s) for the author(s) of this article can be found under https://doi.org/10.1002/srin.202500483.

DOI: 10.1002/srin.202500483

microstructural barriers such as grain boundaries dominate crack initiation, while crack propagation occurs through evolving crack-tip plasticity.[9] In high-cycle fatigue (HCF), cracks typically originate at the surface due to persistent slip bands (PSBs) and microstructural irregularities.[10] In contrast, very HCF (VHCF) conditions, often studied at 20 kHz, can induce subsurface crack initiation due to stress concentration around inclusions.[11] However, in the present study, testing was conducted at 1000 Hz solely as an accelerated method to evaluate fatigue performance following surface treatment, and not to explore VHCF-specific failure mechanisms.

Mechanical and electrochemical surface treatments such as polishing and electropolishing are widely used to remove surface defects and enhance fatigue resistance. Surface removal of 5–10 μm has been shown to delay crack initiation[12,13] yet the efficacy of such treatments in the presence of subsurface damage remains unclear. Additionally, the influence of loading frequency and the lack of fatigue-specific reuse criteria make it difficult to predict how reconditioned components will perform in practical applications.

Despite growing interest in steel reuse, especially in the construction industry,[14] current industrial practices lack standardized methods to quantify surface damage or verify whether surface treatments restore fatigue life sufficiently for safe reuse. In parallel, recent studies have explored additive remanufacturing methods such as wire arc additive manufacturing (WAAM) to restore damaged low-carbon steel components, demonstrating improvements in fatigue and wear performance.[15,16] While such additive approaches offer advantages in geometrical restoration, they are often unsuitable for high-strength steels in fatigue-critical applications where dimensional tolerances are tight and surface integrity is paramount. The present work instead focuses on subtractive surface reconditioning to enhance reusability of such components. In many cases, reuse decisions are made conservatively, without data on the actual residual performance of treated components. Existing approaches typically assess surface quality or fatigue strength in isolation, rarely integrating both within a practical decision-making framework.

This study addresses that gap by quantifying surface fatigue damage through PSB depth analysis, supported by nondestructive diagnostics such as magnetic Barkhausen noise (MBN) and thermographic monitoring. It evaluates mechanical and electrochemical polishing as reconditioning strategies and the reuse potential (RP) metric, which was first presented in our earlier work[17] to assess post-treatment fatigue performance. Using a testing frequency of 1000 Hz for accelerated loading in HCF regime, the methodology enables time-efficient assessment of residual fatigue life. These insights lay the foundation for scalable, diagnostics-based reuse protocols for high-strength steels in fatigue-critical applications, supporting circular economy goals. While this work focuses on a single surface removal depth, the resulting 12-fold recovery in fatigue life underscores the dominant role of surface-driven damage. The framework presented here establishes a validated baseline for future exploration of subsurface effects and treatment optimization.

2. Experimental Section

2.1. Material Selection

The steel grade 42CrMo4 was chosen due to its broad usage in safety-relevant but nonaerospace fatigue applications such as bolts, shafts, and mechanical couplings used in construction, rail transport, and heavy machinery. Its tempered martensitic microstructure provides a relevant platform for evaluating fatigue damage and life extension via surface reconditioning. Moreover, the steel's established mechanical profile supports its suitability as a baseline material for developing reusability frameworks (refer to **Table 1** for chemical composition details).[18]

The material was austenitized at 880 °C for 30 min, then water-quenched to achieve almost complete martensitic transformation before tempering at 550 °C for 90 min to produce fine carbide precipitation and relieve internal (residual) stresses. The heat treatment resulted in Vickers hardness of 375 ± 10 HV10.

2.2. Specimen Preparation for Fatigue Testing

For fatigue experiments, electropolishing was performed on specimens machined according to the geometry given in **Figure 1** to eliminate defects from machining while achieving a consistent surface finish, as described by Polák and Ghanem et al.[13,19] Also, the specimen geometry was optimized for resonance at 1000 Hz based on manufacturer guidelines and validated for each specimen through frequency sweeps prior to testing.

Electropolishing was conducted using electrolyte (Steuers, A2) at 22 V, 2.5–3.0 A, and −10 °C. The process removes surface peaks through anodic dissolution, resulting in a uniform, defect-free finish. Low-temperature control prevents overheating and ensures precise removal of machining artifacts.

Figure 1 illustrates the electropolished fatigue specimen optimized to limit the maximum stress level to its center. It also qualitatively compares the surface quality of the mechanically polished surface and the electropolished surface, which is distinctively visible from the scanning electron microscopy (SEM) images.

2.3. Fatigue Testing and Analysis

The study used a four-phase experimental approach to analyze fatigue behavior while optimizing surface reconditioning methods.

Table 1. Chemical composition of the investigated 42CrMo4 steel as measured by optical emission spectroscopy (OES).

	C	Si	Mn	Mo	P	Cr	S	Fe
wt%[a)]	0.410	0.270	0.780	0.190	0.015	1.020	0.024	Balance

[a)]All concentrations are given in wt.%.

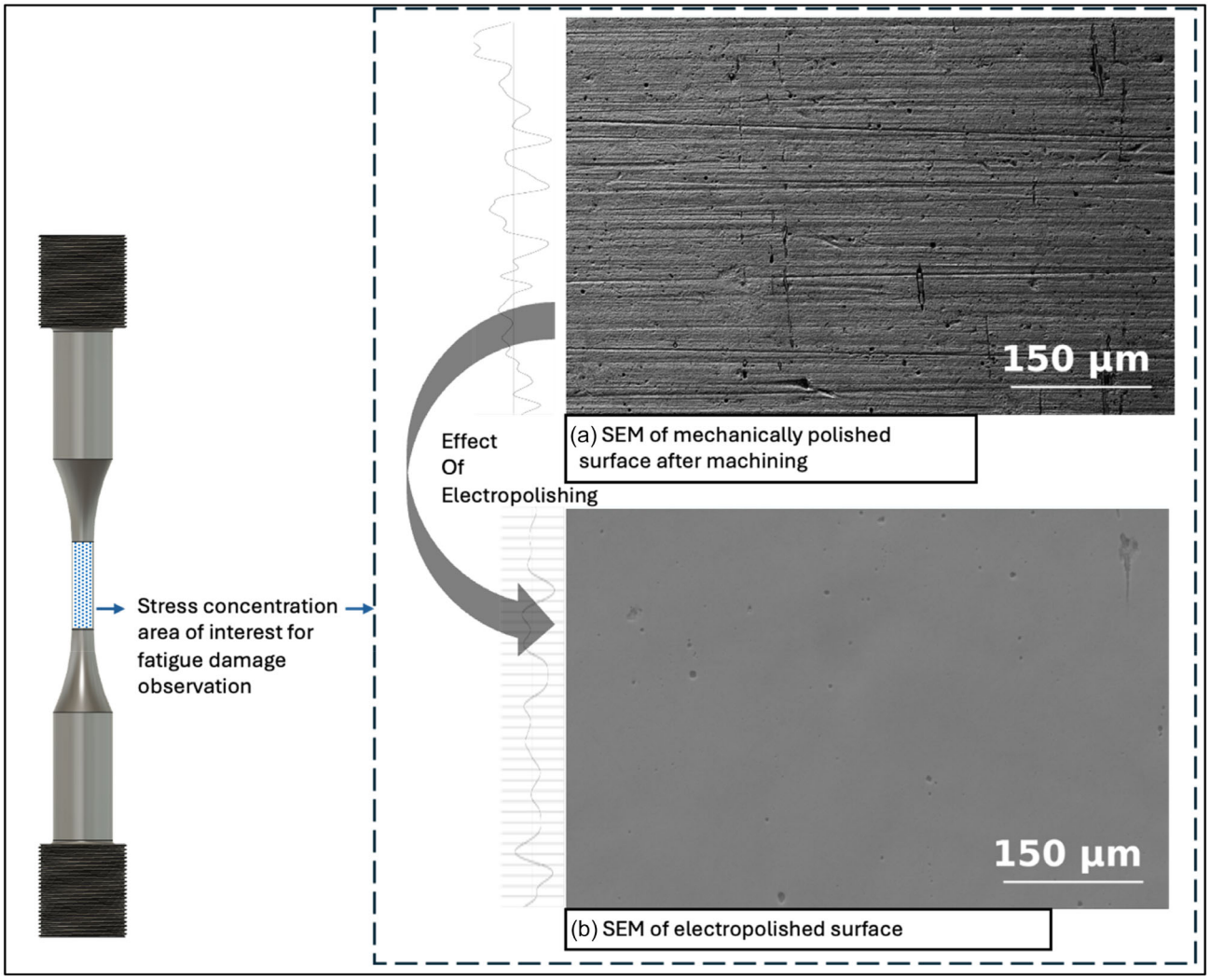

Figure 1. Fatigue specimen with region of interest (left) and SEM images (right) of the a) mechanically polished and b) electropolished surface.

2.3.1. Phase 1: Fatigue Characterization and Predamage Induction via Primary Loading (PL)

Fatigue behavior was initially characterized by constructing S–N curves at two distinct frequencies: 5 and 1000 Hz. These frequencies capture the contrast between standard and accelerated fatigue regimes. Due to test duration and equipment constraints, intermediate frequencies were not included at this stage. However, additional fatigue tests at 260 Hz are planned as part of ongoing work to better characterize frequency-dependent fatigue behavior.

The 5 Hz tests were performed using a servo-hydraulic fatigue testing system (Shimadzu Deutschland GmbH, type EHF-U 50 kN) under fully reversed stress-controlled loading ($R = -1$) with a sinusoidal waveform at room temperature. Mechanical stress–strain hysteresis was monitored using a Dynastrain tactile extensometer with a 15 mm gauge length. The clamps of the 5 Hz testing system were water-cooled, and the temperature gradient between them was kept below 0.5 K to avoid heat transfer into the specimen. For the 1000 Hz tests, a high-frequency resonance fatigue testing system (Russenberger Prüfmaschinen AG, GigaForte 50) was used under the same loading conditions ($R = -1$). Before each high-frequency test, the natural longitudinal resonance frequency of the specimen was identified via a frequency sweep, and the applied loading frequency was tuned accordingly to ensure consistent and accurate dynamic loading. Compressed air cooling was applied during all constant amplitude fatigue tests at 1000 Hz to minimize temperature rise and avoid thermal influence on the results. Temperature evolution during testing was recorded using a thermocouple to identify the fatigue limit. Although no external cooling system was applied during the load increase test (LIT), the thermal response was deliberately monitored to serve as an indicator of material behavior and fatigue damage evolution.

To simulate predamaged conditions, a subset of 5 Hz constant amplitude tests (CATs) was adapted into PL experiments. These tests were interrupted at ≈75% of the estimated fatigue life. A stress amplitude of $\sigma_a = 720$ MPa was selected to induce

reproducible HCF damage without exceeding the macroscopic yield strength of the tempered 42CrMo4 steel. Although prior literature does not explicitly prescribe 1.25 times the fatigue limit as a threshold, previous studies on tempered martensitic steels, including work by Krupp et al.[20] show that loading within 1.2–1.3 times the fatigue limit effectively simulates cyclic microstructural degradation without transitioning to unstable crack growth. The presence of surface fatigue damage under these conditions was further supported through plasma focused ion beam (PFIB) cross-sectioning and MBN analysis.

2.3.2. Phase 2: Damage Investigation due to PL

Damage due to PL was observed in phase 2 using three different techniques-damage observation by SEM, including PFIB milling, electrical resistance measurement, MBN, and thermographic monitoring techniques.

The PFIB system (Thermofisher, PFIB) was used to accurately extract thin lamella from areas showing considerable fatigue damage (**Figure 2**). This technique allows direct observation and measurement of the PSBs in damaged areas by milling cross-sections, which were developed during cyclic loading. The penetration depth and spatial distribution of slip bands were measured to identify the localized plastic deformation and serve as early indicators of crack formation.

Nondestructive testing (NDT) methods consisted of temperature measurements using an infrared (IR) camera (Micro-Epsilon Messtechnik GmbH & Co. KG, type thermoIMAGER TIM QVGA HD) and electrical resistance measurements through the 4-wire method (Toellner, type TOE 7621 power supply). Additionally, ex situ MBN measurements (QASS GmbH, type μmagnetic) result in additional data that can be correlated with material degradation processes based on the detection of permeability changes within the material. These techniques provide a broad understanding of material behavior to develop effective surface reconditioning plans to restore fatigue performance.

2.3.3. Phase 3: Surface Reconditioning

Following the detailed damage assessment during phase 2, the specimens were subjected to targeted mechanical and electrochemical surface reconditioning procedures. These procedures focused on eliminating known surface defects, including PSBs and microcracks, to improve fatigue resistance.

2.3.4. Phase 4: Secondary Loading (SL) and RP Assessment

Following surface reconditioning, the residual fatigue life of PL specimens was evaluated under SL, $\sigma_a = 630$ MPa at 1000 Hz. Compressed air cooling was also used during SL experiments to prevent thermal buildup at 1000 Hz. The SL stress of 630 MPa was then chosen from the HCF regime (just above 10^6 cycles at 1000 Hz frequency S–N curve). This value lies below the yield strength and within the HCF domain, allowing the evaluation of residual fatigue performance postsurface reconditioning.

To assess the effectiveness of surface reconditioning, RP metric, explained in Section 4.3, was used as a dimensionless measure of restored fatigue life. It provides a dimensionless metric for evaluating how much residual life can be recovered through surface treatment techniques.

3. Results

3.1. Microstructure

Light optical microscopy (LOM), SEM, and electron backscatter diffraction (EBSD) were used to characterize the microstructure after the quenching and tempering heat treatment. The LOM image of a 2% Nital-etched specimen (**Figure 3**a) displayed a fine martensitic lath structure with indistinct prior austenite boundaries—typical for tempered martensitic steels. SEM analysis (Figure 3b) provided detailed insights into the morphology and density of martensitic laths. The EBSD inverse pole figure

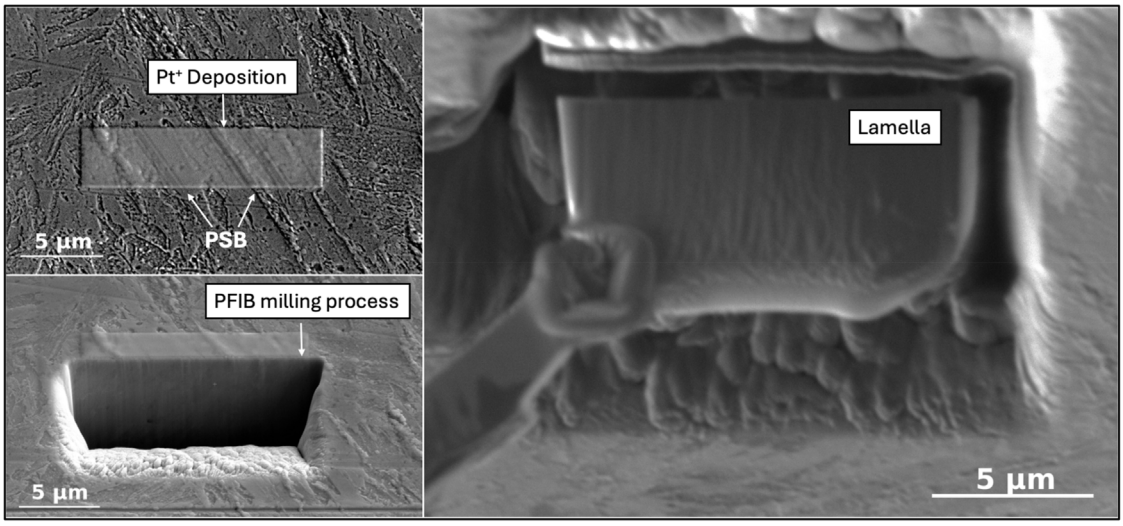

Figure 2. Lamella extraction using PFIB for postfatigue damage identification.

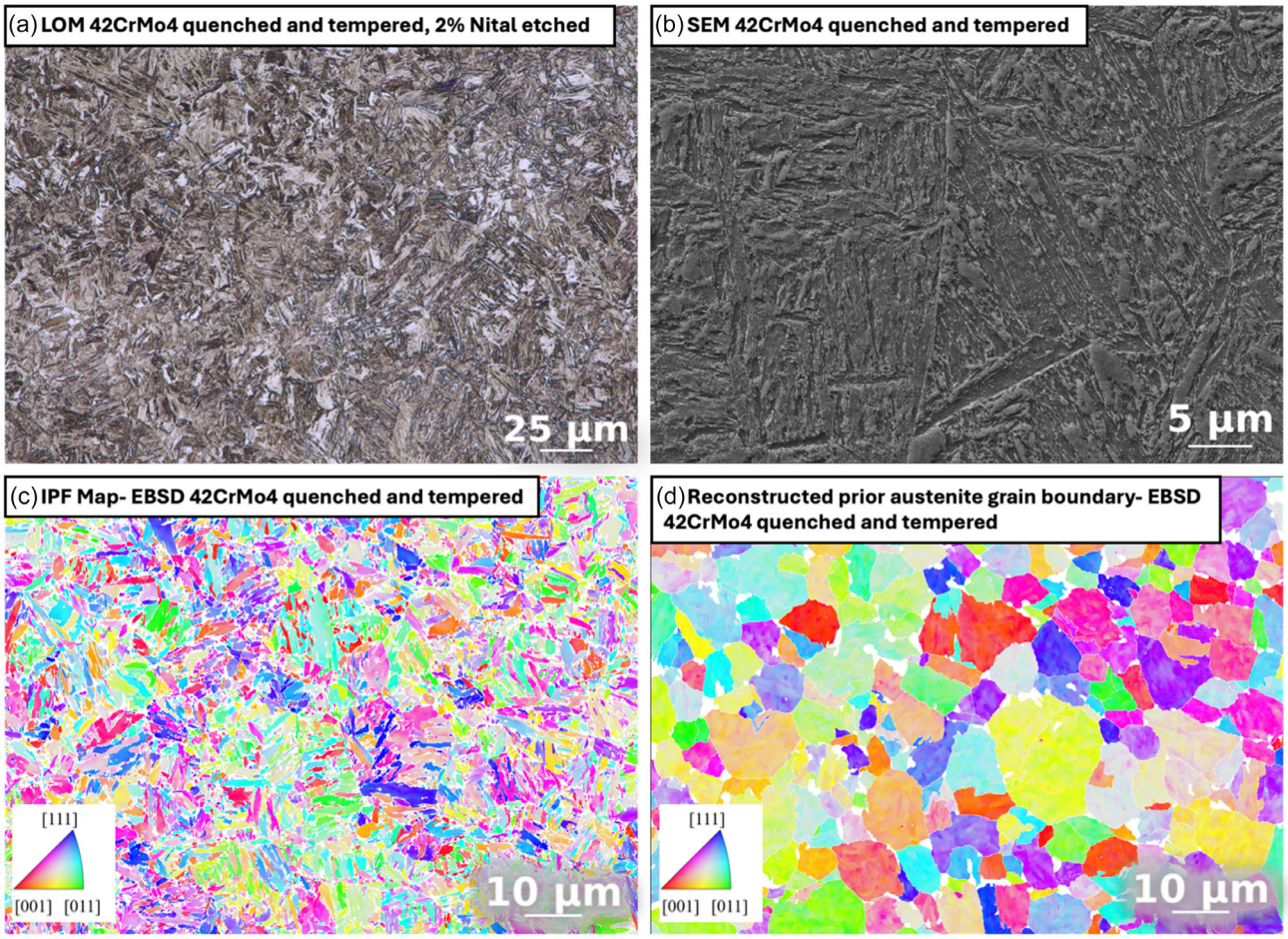

Figure 3. Microstructural analysis of quenched and tempered 42CrMo4 steel: a) LOM image showing etched martensitic laths; b) SEM image highlighting the lath morphology at higher resolution; c) EBSD IPF map showing martensitic packet and block orientations; and d) reconstructed prior austenite grain structure based on EBSD data using the Kurdjumov–Sachs orientation relationship. Reproduced with permission.[17] Copyright 2025, Elsevier.

(IPF) map (Figure 3c) at 10 µm scale revealed the crystallographic orientation of martensite blocks and packets, as well as the presence of high-angle grain boundaries. Using EBSD data and the Kurdjumov–Sachs (K–S) orientation relationship, the prior austenite grain structure was reconstructed (Figure 3d), assuming 24 possible martensitic variants within each prior austenite grain. The analysis yielded an average prior austenite grain size of ≈15 µm, which defines the microstructure of martensitic morphology.

3.2. S-N Curves at 5 and 1000 Hz

Fatigue tests were conducted at 5 and 1000 Hz to investigate the fatigue behavior of quenched and tempered 42CrMo4 steel at different frequencies.

At 5 Hz, a trend S–N curve was generated using the StressLife methodology, a short-term fatigue life assessment approach developed by Starke.[21] This method combines one LIT and CATs with nondestructive measurements to estimate fatigue limit and the S–N curve using only a few specimens. The measured temperature response is decomposed into elastic and plastic parts and evaluated using a generalized Morrow-type formulation to determine fatigue life with reduced experimental effort. Based on this approach, an estimated fatigue strength of 575 MPa was identified (**Figure 4**a), as earlier published by Raghuraman et al.[17]

In contrast, the 1000 Hz S–N curve (Figure 4b) was constructed from conventional failure tests and LIT. The fatigue limit was determined to be 550 MPa, based on the change in slope of the temperature response curve during LIT. This thermal transition marks the onset of considerable microstructural damage accumulation and has been validated in prior high-frequency fatigue studies by Gulbay et al.[22] The specimens surviving beyond 10^7 cycles were treated as runouts. These runouts were noted by open symbols for reference but were not used in a probabilistic fit. The LIT approach allowed a time-efficient determination of the fatigue threshold under controlled thermal conditions.

3.3. PL Induced Damage Assessment

3.3.1. MBN and Change in Temperature as Material Response

The specimens experienced primary cyclic loading at 720 MPa until they reached 75% of their fatigue life with 33 750 cycles

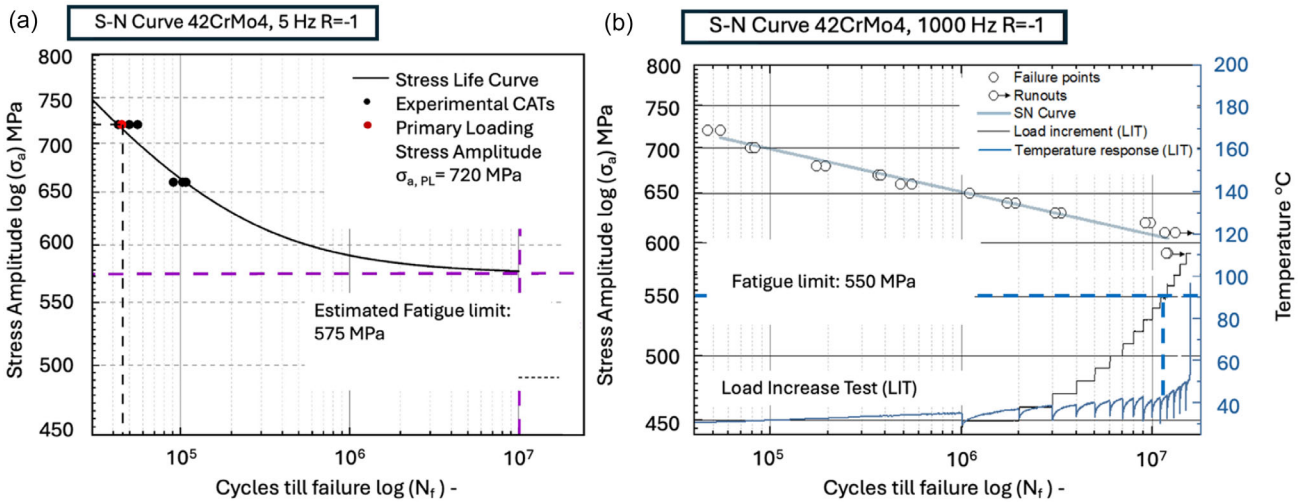

Figure 4. a) 42CrMo4 S–N curves for 5 Hz frequency testing using StressLife method[17] and b) 42CrMo4 S–N curves for 1000 Hz frequency testing using conventional failure method and LIT with corresponding temperature profile. Reproduced with permission.[17] Copyright 2025, Elsevier.

to replicate typical HCF stages. The study investigates the material degradation process using MBN in the initial condition (IC) and after PL, as demonstrated in prior results by Raghuraman et al.[17] **Figure 5** shows that MBN amplitude and surface temperature both increase after PL, indicating magnetic domain activity and internal stress reconfiguration consistent with early fatigue damage, as similarly described by Makowska et al.[23] The responses from these materials provide essential primary quantitative measures of fatigue damage, which help assess the specimen's integrity and potential for reuse.

SEM of Fatigue-Induced Surface Damage: Following PL, SEM examination (**Figure 6**) uncovered extensive surface damage, evident by typical PSBs characteristics (intrusions, extrusions, and microcracks). The observed damage features match well with established fatigue damage mechanisms found in research by Polák et al., highlighting surface conditions as key factors determining fatigue life.[19]

PSB Depth Analysis: Cross-sectional analysis was conducted using SEM on lamella extracted via PFIB milling to investigate subsurface fatigue damage from the PL condition. SEM depth analysis (**Figure 7**) revealed PSBs extending ≈5 µm below the material surface. The high-resolution image also captured surface intrusions and extrusions along PSB paths, along with evidence of void nucleation and short crack formation just underneath the surface.

Additionally, areas with varying dislocation densities—indicative of concentrated plastic deformation beneath the surface—were observed, aligning well with studies by Polák et al.[10,19,24] These subsurface deformation features, including the transition from slip localization to crack initiation, emphasize the critical role of PSBs in early-stage fatigue damage. PFIB-assisted cross-sectional SEM imaging proves essential in assessing PSB-induced degradation and guiding surface reconditioning strategies for fatigue life extension and RP.

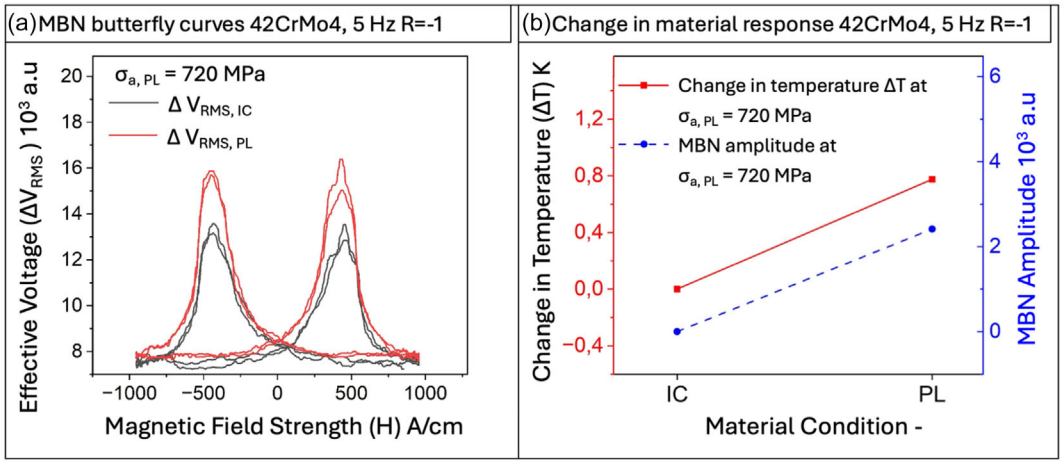

Figure 5. MBN and thermographic response of 42CrMo4 steel before and after PL at $\sigma_a = 720$ MPa: a) MBN butterfly curves showing shifts in effective voltage as a function of magnetic field strength, comparing the IC and PL states and b) Change in surface temperature (ΔT) and MBN amplitude between IC and PL, revealing quantifiable degradation following 75% of estimated fatigue life. Reproduced with permission.[17] Copyright 2025, Elsevier.

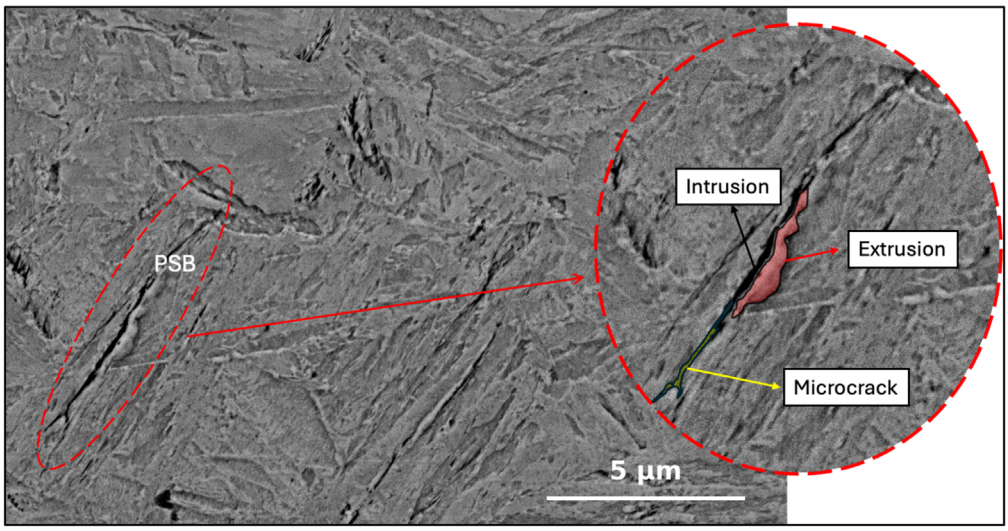

Figure 6. SEM images exhibiting typical PSB and fatigue surface damage (extrusion, intrusion, and microcrack) resulting from PL.

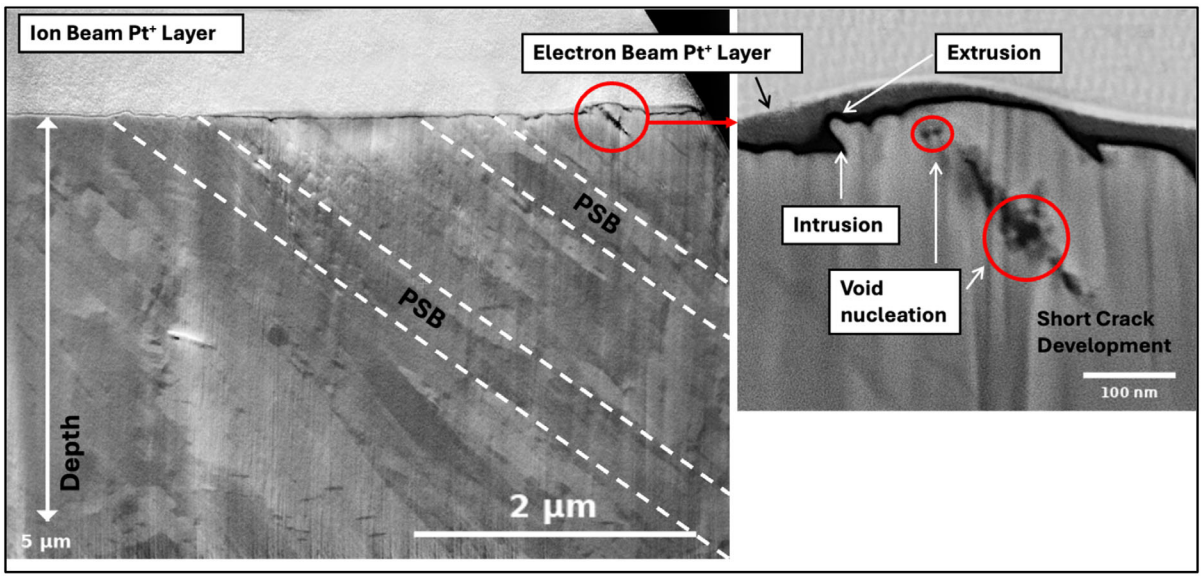

Figure 7. High-resolution SEM image of a PFIB-milled lamella from the PL condition, showing PSBs extending ≈5 µm below the surface. Localized surface intrusions, extrusions, void nucleation, and early crack formation highlight the onset of fatigue damage.

3.4. Improved Fatigue Life via Surface Reconditioning

Although PSBs were visibly observed at ≈5 µm depth, the decision to remove 100 µm was guided by prior studies from Murakami and Haghshenas et al., which demonstrate that subsurface fatigue-induced damage frequently extends significantly deeper than surface-visible features.[11,13] This conservative removal ensures mitigation of hidden crack initiation sites. Surface reconditioning, combining mechanical polishing and electropolishing, was used to eliminate fatigue damage resulting from PL at 720 MPa.

Figure 8 presents a comparative analysis of fatigue life under SL at 630 MPa for reference-state, reconditioned, and nonreconditioned specimens. Reconditioned specimens achieved a substantial improvement ($\approx 1.06 \times 10^6$ cycles) compared to untreated ones ($\approx 8.5 \times 10^4$ cycles), clearly demonstrating the effectiveness of the surface reconditioning protocol. However, reconditioned specimens did not fully recover to the reference-state fatigue life ($\approx 2.9 \times 10^6$ cycles), likely due to residual volume damage beyond the reach of surface removal. These results were also published in earlier studies by Raghuraman et al.[17]

Each condition was tested using 3–5 specimens to identify relative fatigue trends and to ensure repeatability of results. While the sample size limits statistical generalization, it aligns with established practice for preliminary studies focused on identifying relative fatigue trends. Gui et al. showed that fatigue crack initiation in bainite/martensite steels can arise from subsurface microstructures and exhibit wide scatter due to local phase

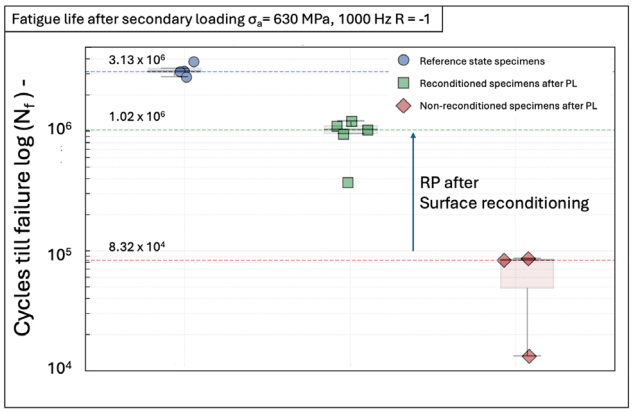

Figure 8. Fatigue life comparison for reconditioned versus nonreconditioned specimens depicting the gain in RP due to surface reconditioning. Reproduced with permission.[17] Copyright 2025, Elsevier.

heterogeneity and prior austenite grain variation.[25] Similarly, Giertler and Krupp demonstrated that microcracks are often arrested or deflected by grain boundaries, and crack propagation becomes highly sensitive to local crystallographic misorientation.[26] These mechanisms, particularly relevant under VHCF conditions, explain the variation in observed fatigue life and further support the microstructure-sensitive nature of fatigue behavior in reconditioned steels.

3.5. Fractographic Analysis

Fractographic analysis was performed on selected reconditioned specimens tested under SL at 630 MPa and 1000 Hz. As shown in **Figure 9**, examined samples exhibited surface-initiated cracks with morphology typical of HCF, such as radial markings and the absence of fine granular areas (FGAs) or fish-eye features associated with VHCF. Even when nonmetallic inclusions were located near the initiation sites, cracking consistently originated at the surface, indicating they did not act as dominant flaws after reconditioning.

The observed scatter in fatigue life is consistent with prior findings for martensitic steels, where microstructural heterogeneity such as variations in packet orientation or boundary density can locally influence crack initiation. Although a direct correlation between fatigue life and specific microstructural features was not established in this study, the relatively narrow scatter range observed suggests that the tested steel's tempered martensitic microstructure provides consistent resistance to surface-driven fatigue mechanisms under both 5 and 1000 Hz loading.

4. Discussion

4.1. Frequency Effect on S-N Curve

The comparison of S–N curves at frequencies of 5 and 1000 Hz (Figure 4) highlights a subtle frequency-dependent behavior in the fatigue limit regime for 42CrMo4 steel. At 5 Hz, the fatigue limit was estimated at ≈575 MPa using a StressLife approach based on two CATs, one LIT, and the corresponding material response relationship. In contrast, the fatigue limit at 1000 Hz was determined to be around 550 MPa through conventional fatigue testing, involving failure experiments. Although derived from fundamentally different experimental procedures, both results converge within a narrow margin, indicating that the frequency effect on fatigue limit is minor under the current heat treatment condition. However, given the distinct testing methodologies, direct equivalence must be interpreted with caution.

The minimal difference observed in fatigue limits between 5 and 1000 Hz can be partly attributed to the strain rate insensitivity of tempered martensitic steels. Prior studies by Krupp and Giertler[27] and Jeddi and Palin-Luc[28] have demonstrated that such microstructures exhibit strong resistance to dislocation motion and localized plasticity, which suppresses frequency-dependent effects like crack-closure.

Although VHCF-related internal crack initiation can occur at high frequencies, such transitions typically require stress amplitudes far below the HCF regime and lifetimes beyond 10^7 cycles. In contrast, all tests in this study remained within the HCF domain. The consistent observation of surface-initiated fractures

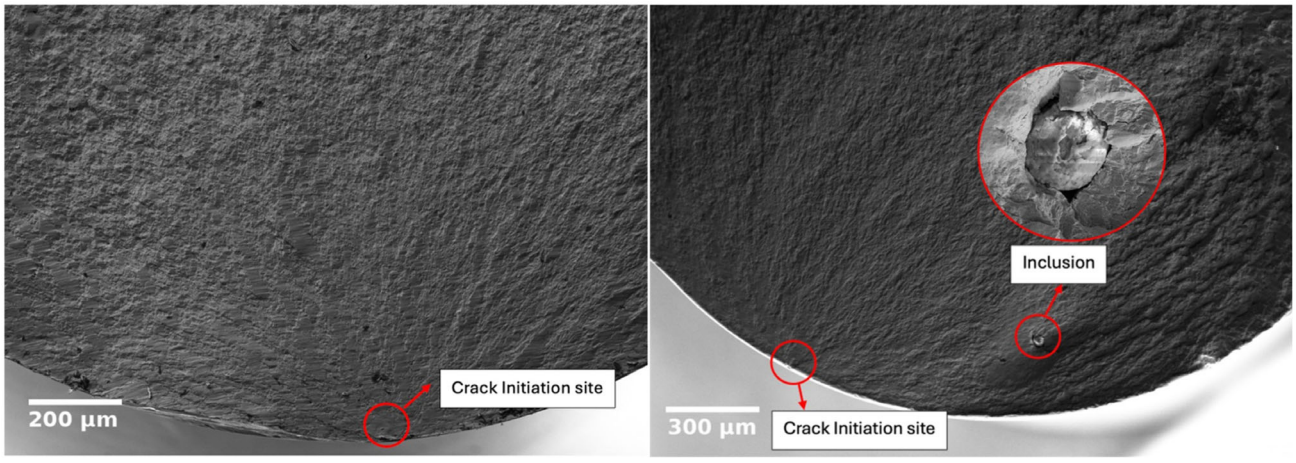

Figure 9. Representative SEM fracture surface images from reconditioned samples after SL. (Left) Failure initiated at the surface in the absence of inclusions. (Right) Surface-initiated crack despite proximity to a noncritical inclusion.

at 1000 Hz (even in specimens containing inclusions) demonstrates that the dominant failure mode remained surface-driven. This strongly supports the conclusion that frequency, under the current test conditions, did not alter the primary damage mechanism.

Damage characterization during PL at 5 Hz using thermography, MBN, and PFIB revealed hallmark features of early surface fatigue, such as PSB formation and microcracks. Despite the absence of direct diagnostics at 1000 Hz, the agreement in fatigue lives, fracture morphologies, and crack initiation sites between the two frequency regimes suggests a continuity in damage evolution. This continuity justifies the use of 5 Hz signal interpretations (e.g., MBN and thermography) as representative indicators for surface damage assessment, even under high-frequency SL.

While surface temperatures during 1000 Hz testing reached up to 130 °C, no thermal degradation or subsurface failure features were observed. The data indicate that the tempered martensitic microstructure exhibits sufficient thermal and mechanical robustness to withstand localized heating without altering the fatigue behavior in the studied regime.

4.2. Surface Removal Strategy, Diagnostics, and Real-World Applicability

A study from Polák shows that PSBs cause localized cyclic plasticity, forming persistent slip markings (PSMs) with extrusions and intrusions, as observed in Figure 5.[24] Deep intrusions act as crack-like defects that can initiate intragranular fatigue cracks. Multiple PSMs may form along grain boundaries, where intrusions serve as crack embryos and extrusions stress adjacent grains, leading to shallow boundary cracks. These are influenced by the cyclic yield stress mismatch between the matrix and PSBs. This highlights the importance of surface removal to address the damage control due to PL.

Moreover, precise PSB penetration depth measurement remains essential because these bands consist of microstructural areas with significant cyclic plastic behavior, which affects fatigue crack evolution, as outlined by Krupp.[29] Also, research by Peralta et al. demonstrated that PSBs are responsible for transforming microstructural fatigue damage into visible cracks beyond just their initial formation stage.[30] Their research demonstrated that PSBs saturate the strain energy and enable microcrack coalescence during HCF, thus confirming the depth-dependent findings of this study.

Although PSBs were found at depths of ≈5 μm, the actual extent of fatigue damage may reach beyond the visible zone, especially in components subjected to prolonged or multiaxial service loads. The removal of 100 μm was chosen conservatively, but future studies will investigate fatigue performance after varied surface removal depths (e.g., 10, 50, and 150 μm) to establish optimal thresholds. This will be supported by PFIB and NDT techniques such as MBN to evaluate residual damage. These efforts aim to better quantify the limits of reconditioning in the presence of incipient subsurface cracks.

To determine optimal surface removal depth for life extension, a data-informed, nondestructive evaluation (NDE) guided approach is essential. While this study applied a conservative 100 μm removal based on prior fatigue studies, future strategies should quantify damage gradients using methods such as MBN and thermography after incremental removal steps. Although postremoval MBN assessments were not conducted in this study, they remain a promising approach for verifying return-to-baseline magnetic response after reconditioning. In operational practice, complementary NDT methods such as alternating current field measurement, eddy current testing, and magnetic flux leakage are widely applied in the rail and railway-wheel sectors for crack detection, residual-stress evaluation, and wheel-burn identification. These methods are often embedded within structured maintenance-planning frameworks, for example, preventive grinding schedules and life-cycle-cost-based intervention programs to detect and remove fatigue damage before failure. Adapting such diagnostics-guided maintenance strategies to high-strength steel components outside the rail sector offers a practical pathway to verify reconditioning effectiveness and to set quantitative pass/fail criteria for reuse. For recent overviews and methodology examples, see Ekberg et al.[31] and Nia et al.[32] Also, MBN's sensitivity to stress and dislocation density has been correlated to early fatigue damage depths in gear steels and railway components, enabling its potential use as a damage-monitoring technique. Coupling MBN with PFIB-based microstructural insights can support quantitative decisions about when intervention is most effective, especially if removal thresholds can be linked to changes in magnetic response. In real-world scenarios, economic and logistical constraints often preclude frequent inspection; therefore, intervention may be best positioned either after predefined service intervals or toward the end-of-life, particularly when component history is uncertain. This usually comes with a trade-off between the damage induced and the efforts to apply the reuse strategy. The use of surface reconditioning promotes not only life extension but also a final-stage reuse. However, warranty implications and sector-specific safety regulations must be integrated into such reuse frameworks to ensure compliance and user trust.

4.3. RP Calculation Incorporating Frequency Effects

The fatigue life improvement from 8.32×10^4 to 1.02×10^6 cycles achieved through targeted surface polishing directly validates the effectiveness of the proposed reconditioning protocol. This 12.25-fold increase in endurance highlights the dominant role of surface-initiated damage in fatigue failure and confirms that its removal can meaningfully extend service life, even under high-frequency loading.

The RP metric, first introduced in our earlier work,[17] is applied here to provide a practical, quantifiable measure of reuse feasibility. By comparing postreconditioning life to both unmodified and reference conditions, it contextualizes the sustainability and performance trade-offs. Although complete recovery to reference endurance (3.13×10^6 cycles) was not achieved, the residual deficit is attributed to subsurface fatigue evolution initiated during the primary load phase. Nevertheless, the possibilities of suppressing surface-driven mechanisms alone were sufficient to secure a significant reuse window.

These findings argue that surface polishing, guided by nondestructive diagnostics (e.g., MBN or thermography), can be used

to selectively rehabilitate fatigue-exposed steel components, particularly in nonaerospace sectors where full replacement is economically or logistically impractical.

To evaluate the effectiveness of the proposed reconditioning strategy, a RP metric was introduced as a normalized measure of restored fatigue life

$$\mathrm{RP} = \frac{N_\mathrm{f}^\mathrm{SL}}{N_\mathrm{f}^\mathrm{PL}} \tag{1}$$

where N_f^SL is the fatigue life achieved during the second loading phase after reconditioning, and N_f^PL is the life recorded during the PL prior to reconditioning.

Additionally, a reference-normalized form of RP was introduced to assess how closely the reconditioned surface approaches the performance of pristine specimens

$$\mathrm{RP}^* = \frac{N_\mathrm{f}^\mathrm{SL}}{N_\mathrm{f}^\mathrm{ref.}} \tag{2}$$

In this study, RP was calculated to be 12.25, and RP* ≈0.33, indicating that although full restoration was not achieved, a substantial portion of the original endurance limit was recovered (**Table 2**).

Fractographic analysis supports these quantitative trends. Despite high-frequency loading and the presence of inclusions in some cases, crack initiation in reconditioned specimens remained surface-driven. No signs of subsurface or VHCF-type failures were observed, reinforcing the interpretation that the removal of surface damage was the primary driver of fatigue life extension.

Despite the clear improvement from surface treatment with mechanical and electropolishing, the reconditioned specimens did not fully recover to the baseline fatigue life of pristine samples. This residual deficit likely originates from volume-localized damage mechanisms initiated during PL, such as early-stage microcracks or subsurface dislocation structures that are not fully removed by surface treatments alone. To further enhance fatigue life recovery, hybrid approaches such as deep mechanical polishing, laser shock peening, or low-temperature annealing could be explored. These techniques may help relax internal stresses or arrest incipient subsurface damage without compromising the core microstructure.

Regulatory frameworks in high-risk sectors such as aerospace currently restrict the reuse of fatigue-exposed components. However, the methodology proposed in this study offers a structured foundation for condition-based reuse in industrial contexts. Specifically, components nearing the end of their nominal service life, such as those used in construction, heavy machinery, or rail systems, can be evaluated for surface-initiated fatigue damage using NDT methods, as detailed in Section 4.2, to verify surface condition prior to reconditioning. If damage indicators such as PSB intrusions, thermographic hotspots, or MBN signal shifts remain below empirically established thresholds (e.g., intrusion depths below 2 µm, no subsurface cracking in SEM cross-sections, or signal profiles consistent with precritical fatigue exposure), surface material can be selectively removed through mechanical or electrochemical polishing to restore integrity. Implementing this strategy on an industrial scale would require integration into sector-specific safety audits, certification protocols, and traceable documentation systems. By focusing on measurable surface damage criteria, this reuse strategy offers a feasible bridge between laboratory insights and practical deployment in the circular use of high-strength steels.

Table 2. Fatigue life and RP for reference, as-damaged, and reconditioned specimens.

Condition	Fatigue life (Cycles)	RP versus As-damaged	RP versus Reference
Reference (no damage)	3.13×10^6	–	1.00
As-damaged (no reconditioning)	8.32×10^4	1.00	0.027
After reconditioning	1.02×10^6	**12.25**	**0.33**

5. Summary

This study establishes a systematic framework to evaluate the RP of prefatigued 42CrMo4 steel by integrating multifrequency fatigue testing, surface damage diagnostics, and reconditioning strategies. Predamaged specimens underwent cyclic loading at 720 MPa and 5 Hz to simulate controlled HCF exposure (75% of fatigue life), followed by targeted material removal (≈100 µm) via mechanical and electrochemical polishing.

Fatigue behavior was characterized through S–N curves at 5 and 1000 Hz, constructed using the StressLife approach and high-frequency resonance testing, respectively. Post reconditioning, SL tests at 630 MPa and 1000 Hz revealed a fatigue life extension from 8.32×10^4 to 1.02×10^6 cycles, corresponding to a 12.25-fold increase. This substantial gain confirms that surface-initiated fatigue mechanisms (primarily PSBs and microcracks, as verified via PFIB and SEM) are the dominant life-limiting factors and can be effectively mitigated through precision surface treatments.

The RP metric originally introduced in our earlier work[17] serves as a robust, dimensionless indicator to quantify reusability relative to baseline and reference life. While full recovery to the undegraded reference state (averaged 3.13×10^6 cycles) was not achieved, the pronounced life restoration underscores the feasibility of reusing fatigue-exposed components through surface-focused interventions. This approach enables informed decision-making in sustainability-driven applications, particularly under high-frequency HCF conditions.

Future work will target the evaluation of subsurface damage beyond the observed 5 µm PSB depth and explore advanced surface and thermal treatments such as shot peening, laser shock peening, or postfatigue annealing, as demonstrated by Saklakoglu et al.,[33] to enhance both surface and volumetric fatigue resistance in reuse-critical applications. While the present study is limited to laboratory-scale specimens, it establishes a validated foundation for extending this methodology to real-world components. Upcoming efforts will include large-scale specimens with application-relevant geometries to assess the performance of reconditioning strategies under operational loading conditions. Additionally, a combination of variable-depth removal and NDE-guided diagnostics will be implemented to improve decision-making robustness and industrial adaptability. Collectively, these developments aim to bridge the gap between laboratory validation and scalable deployment for the reuse of structural steel components.

Acknowledgements

The authors express their gratitude to the German Research Foundation (DFG), whose joint project funding (502121294) enabled this research. The authors extend special appreciation to Jens Ludwig for his technical expertise and dedicated assistance at IEHK, which played a crucial role in executing numerous experiments successfully.

Open Access funding enabled and organized by Projekt DEAL.

Conflict of Interest

The authors declare no conflict of interest.

Author Contributions

Ayush Shrivastava: investigation (lead); methodology (lead); writing—original draft (lead). **Oguz Gulbay**: writing—review & editing (supporting). **Srinivasa Raghavan Raghuraman**: investigation (supporting); writing—review & editing (supporting). **Marion Kreins**: data curation (supporting); supervision (supporting); writing—review & editing (supporting). **Fabian Weber**: supervision (supporting); writing—review & editing (supporting). **Peter Starke**: supervision (supporting); writing—review & editing (supporting). **Alexander Gramlich**: conceptualization (supporting); supervision (supporting); writing—review & editing (supporting). **Ulrich Krupp**: conceptualization (lead); supervision (lead); validation (lead); writing—review & editing (lead).

Data Availability Statement

The data that support the findings of this study are available from the corresponding author upon reasonable request.

Keywords

42CrMo4 steel, fatigue damage, high cycle fatigue, non-destructive testing, reuse potential, surface reconditioning

Received: May 16, 2025
Revised: August 15, 2025
Published online:

[1] V. G. Lisienko, A. V. Lapteva, Y. N. Chesnokov, *Steel Transl.* **2015**, *45*, 623.
[2] *Iron and Steel Technology Roadmap*, IEA, Paris, France **2020**.
[3] J. Berglund-Brown, *Structural Steel Reuse as a Cost-Effective Carbon Mitigation Strategy, Master's Thesis*, Massachusetts Institute of Technology, Cambridge, MA, USA **2023**.
[4] D. Raabe, M. Jovičević-Klug, D. Ponge, A. Gramlich, A. K. Silva, A. N. da, Grundy, Y. Ma, *Annu. Rev. Mater. Res.* **2024**, *54*, 247.
[5] D. D. Tingley, S. Cooper, J. Cullen, *Understanding and Overcoming the Barriers to Structural Steel Reuse: A UK Perspective*, Research Report **2016**, https://doi.org/10.13140/RG.2.1.2162.7766.
[6] M. Gorgolewski, *Build. Res. Inf.* **2008**, *36*, 175.
[7] S. Mao, W.-J. Cao, in *IABSE Congr. Rep.*, San José, Cost Rica **2024**, 25–27.
[8] D. Cooper, A. C. Skelton, M. C. Moynihan, J. M. Allwood, *Resour. Conserv. Recycl.* **2014**, *84*, 24.
[9] J. Schijve, *Fatigue of Structures and Materials*, Springer, Dordrecht, The Netherlands **2009**.
[10] J. Polák, T. Lepistö, P. Kettunen, *Mater. Sci. Eng.* **1985**, *74*, 85.
[11] Y. Murakami, T. Endo, *Int. J. Fatigue* **1980**, *2*, 23.
[12] F. Ghanem, N. B. Fredj, H. Sidhom, *Int. J. Adv. Manuf. Technol.* **2011**, *52*, 583.
[13] A. Haghshenas, M. M. Khonsari, *Theor. Appl. Fract. Mech.* **2019**, *103*, 102248.
[14] H. Bartsch, F. Eyben, M. Feldmann, in *Nordic Steel Construction Conf.*, Luleå tekniska universitet, Sweden **2024**.
[15] K. Kanishka, B. Acherjee, *Mater. Today Commun.* **2025**, *43*, 111802.
[16] K. Kanishka, B. Acherjee, C. Rahul, P. Anand, *Phys. Scr.* **2024**, *99*, 105601.
[17] S. R. Raghuraman, A. Shrivastava, F. Weber, A. Gramlich, U. Krupp, P. Starke, *Procedia Struct. Integrity* **2025**, *68*, 769.
[18] M. Bayrak, F. Öztürk, M. Demirezen, Z. Evis, *J. Mater. Eng. Perform.* **2007**, *16*, 597.
[19] J. Polák, V. Mazánová, M. Heczko, I. Kuběna, J. Man, *Fatigue Fract. Eng. Mater. Struct.* **2017**, *40*, 1101.
[20] U. Krupp, A. Giertler, K. Koschella, *Procedia Eng.* **2016**, *160*, 231.
[21] P. Starke, *Mater. Test.* **2019**, *61*, 297.
[22] O. Gulbay, M. Ackermann, A. Gramlich, A. R. Durmaz, I. Steinbach, U. Krupp, *Steel Res. Int.* **2023**, *94*, 2300238.
[23] K. Makowska, T. Szymczak, R. Kowalewski, *Acta Mech. Autom.* **2024**, *18*, 40.
[24] J. Polák, *Crystals* **2023**, *13*, 220.
[25] X. Gui, G. Gao, B. An, R. D. K. Misra, B. Bai, *Mater. Sci. Eng. A* **2021**, *803*, 140692.
[26] A. Giertler, U. Krupp, *Procedia Struct. Integr.* **2016**, *2*, 1207.
[27] U. Krupp, A. Giertler, *Metals* **2022**, *12*, 1815.
[28] D. Jeddi, T. Palin-Luc, *Fatigue Fract. Eng. Mater. Struct.* **2018**, *41*, 969.
[29] U. Krupp, *Fatigue Crack Propagation in Metals and Alloys: Microstructural Aspects and Modelling Concepts*, Wiley-VCH, Weinheim, Germany **2007**.
[30] P. Peralta, C. Laird, U. Ramamurty, S. Suresh, G. H. Campbell, W. E. King, T. E. Mitchell, *Fatigue Crack Nucleation in Metallic Materials, Small Fatigue Cracks: Mechanics, Mechanisms, and Applications*, Technical Report (**1999**).
[31] A. Ekberg, E. Kabo, R. Lund'en, *Wear* **2023**, *526–527*, 204891.
[32] S. H. Nia, V. V. Krishna, K. Odolinski, P. T. Torstensson, A. Ait-Ali, L. Sundholm, P.-O. L. Kr aik, S. Stichel, *Wear* **2023**, *532–533*, 205120.
[33] N. Saklakoglu, A. Bolouri, S. G. Irizalp, *Int. J. Adv. Manuf. Technol.* **2021**, *112*, 2961.